Optical conductivity in the vicinity of a quantum critical point

Patrick Bogdanski,[1] Mohammed Halaoui,[1] Andrzej M. Oleś,[2] and Raymond Frésard[1]
[1]*Laboratoire CRISMAT, UMR CNRS-ENSICAEN (ISMRA) 6508, and IRMA, FR3095 Caen, France*
[2]*Marian Smoluchowski Institute of Physics, Jagellonian University, Reymonta 4, PL-30059 Kraków, Poland*
(Received 5 May 2010; revised manuscript received 21 September 2010; published 18 November 2010)

We demonstrate an interrelation between the magnetic properties and optical conductivity $\sigma(\omega)$ for $3d$ electron systems with active orbital degree of freedom at a transition-metal ion: t_{2g} in d^1 and e_g in d^7 configuration. Both systems are described within the two-band Hubbard model which we analyze using exact-diagonalization technique for a two-site molecule at quarter filling. We highlight the main features of the low-temperature optical conductivity spectra for e_g and t_{2g} electrons, in the presence of the crystal-field splitting and show that these spectra provide a way to determine both Hund's exchange J_H and intraorbital Coulomb interaction U. The orbital polarization and the entanglement between spin and orbital degrees of freedom are also discussed, together with possible violations of the Goodenough-Kanamori rules.

DOI: 10.1103/PhysRevB.82.195125 PACS number(s): 75.10.Lp, 72.80.Ga, 75.25.Dk, 78.20.Bh

I. INTRODUCTION

Interest in strongly correlated electron systems keeps on increasing, fueled both by fundamental issues and applications. The need to accurately characterize these systems also leads to a broad range of new very sensitive and comprehensive experiments, the results of which are calling for better interpretation of the experimental data. With that purpose, a promising tool is provided by the local-density approximation (LDA) combined with the dynamical mean-field theory (DMFT), so-called LDA+DMFT approach.[1] It has been successfully applied to a variety of situations, including the celebrated Mott transition in V_2O_3,[2–4] magnetic and orbital ordering in various perovskites, see, e.g., Ref. 5, the negative thermal expansion of δ-Pu,[6] to quote a few. Though mostly *ab initio*, the computed quantities depend in strongly correlated materials on external parameters, such as the Hubbard U or Hund's exchange coupling J_H. As the LDA+DMFT scheme is not devised to determine them, they are typically estimated from experiment.

For example, one uses data resulting from spectroscopy[7] performed on NiO to estimate these parameters for the layered nickelates La_2NiO_4.[8] This, however, keeps an empirical flavor, especially since the DMFT needs to be supplemented by bare parameter values, while experiment provides the renormalized ones, and the relationship among them is not systematically mastered. A possible route to overcome this difficulty consists in optimizing these parameters in order to improve the agreement with experiment but as the calculations are rather involved this does not turn very convenient. Thus extracting the parameters U and J_H from experimental data by means of analytical expressions (or using simple numerical tools) is expected to help improving common understanding of the modeling of strongly correlated systems. This is the goal of the paper. While this is an ambitious task in general, we argue that useful insight can be gained by studying simpler problems, namely, when only a few bands cross the Fermi energy.

With that aim, one quickly notices that multiband Hubbard Hamiltonians can cover a wealth of situations,[9] even when restricting the number of bands (i.e., active $3d$ states per site) to two.[10–13] The anisotropic degenerate two-orbital Hubbard model was studied within DMFT at low temperatures[14] and it was established that the orbital-selective Mott transition occurs in a broad parameter regime.[15] A recent investigation of the orbital-selective Mott transition using the dynamical cluster approximation combined with a continuous-time quantum Monte Carlo algorithm confirmed that this transition is stabilized at half filling.[16] However, at quarter filling a band insulator state for both orbitals is stabilized instead at low temperatures. For a metallic system close to quarter filling it was shown that a heavy quasiparticle band is formed by the Hubbard interaction with the effective mass being only weakly dependent on the orbital splitting and Hund's exchange coupling.[14] Importance of Hund's exchange at quarter filling has also been emphasized recently using the cellular DMFT.[17] While the models studied in this context until now conserve the orbital flavor and are thus designed to describe t_{2g} electrons, the orbital flavor is not conserved for e_g electrons,[18] and one may expect that the magnetic properties and excitations are different. In addition, their response to a (an additional) symmetry breaking term in the orbital space representing the crystal-field splitting (CFS) may differ as well.

Various aspects of the physics of the quarter-filling case have already been studied, either by exact diagonalization,[19] or on the mean-field level,[8,10,20] pointing toward a rich phase diagram, especially for the square lattice. Indeed, for vanishing CFS and large J_H, weak-coupling approach predicts the leading instability to be toward a C-type antiferromagnetic (AF) phase, while for small J_H a homogeneous ferromagnetic (FM) ground state is favored.[10] On the contrary, strong-coupling expansion leading to the celebrated Goodenough-Kanamori rules[21] point toward a staggered FM ground state for large J_H, in agreement with the mean-field results. However, under certain circumstances the Goodenough-Kanamori rules are violated in spin-orbital systems and the spin-orbital entanglement takes place.[22]

The purpose of this paper is to extract generic properties of e_g and t_{2g} electrons in the itinerant regime, where charge fluctuations are still allowed but gradually decrease under increasing electron correlations. The correlations depend on the ratio between the intraorbital Coulomb interaction U and

the hopping element t. The first of the models considered here is the widely used doubly degenerate Hubbard model which, as we explain, stands also for t_{2g} electrons while the second one describes e_g electrons. Investigating these models we focus on: (i) increasing local moments and intersite spin and orbital correlations, and (ii) the interplay between the magnetic ground state and the optical spectra, when the ratio U/t is increased. As we show, the optical spectra are determined by the actual interaction parameters which can be therefore deduced from the charge excitations to the upper Hubbard bands measured in the optical spectroscopy.[23] We shall also investigate the dependence of magnetic correlations on the CFS and show that the boundaries between magnetic phases strongly depend on the actual CFS. Finally, we provide another example of the spin-orbital entanglement and violation of the Goodenough-Kanamori rules in the regime of parameters where this appears surprising and was not expected before.[22]

The paper is organized as follows. The models for t_{2g} and e_g electrons are introduced in Sec. II. In Sec. III we analyze the consequences of Hund's exchange and the CFS on the properties of the system. First, the spectra of the Hamiltonians are presented in Sec. III A. Next we analyze and discuss the magnetic phase diagrams in Sec. III B and the orbital polarization in Sec. III C. We then turn to the optical spectra, and show in Sec. IV that the energies of the optical excitations (at $\omega \simeq U$) are strongly influenced by the magnetic ground state and we determine their characteristic energies analytically. We also discuss the temperature dependence of the spin autocorrelation function in Sec. V. With the orbital autocorrelation function and the entanglement of both spin and orbital degrees of freedom presented in Sec. VI, we show a case of clear violation of the Goodenough-Kanamori rules. A short summary and conclusions are presented in Sec. VII.

II. MODEL HAMILTONIAN FOR e_g AND t_{2g} ORBITALS

Most intriguing properties of transition-metal oxides are ruled by strongly interacting d electrons, which can be found in either t_{2g} or e_g orbitals. Besides, the geometrical environment of the transition-metal ion plays a key role. Accordingly we consider Hamiltonians consisting of three contributions which read as follows:

$$\mathcal{H} = H_{\rm kin} + H_{\rm int} + H_{\rm cf}. \tag{2.1}$$

The first contribution corresponds to the kinetic energy, the second one to the electron-electron interaction, and the last one stands for the often neglected CFS. More specifically, when considering a model involving orbital degeneracy, the kinetic energy is described by

$$H_{\rm kin} = \sum_{\langle ij \rangle} \sum_{\alpha\beta\sigma} t_{ij}^{\alpha\beta} c_{i\alpha\sigma}^{\dagger} c_{j\beta\sigma}, \tag{2.2}$$

where $c_{i\alpha\sigma}^{\dagger}$ is the respective electron creation operator with spin σ in orbital α at site i. The structure of the hopping matrix $t_{ij}^{\alpha\beta}$ depends on the orbitals one is considering, direction in the cubic lattice, and on system dimension. For e_g electrons one may introduce a basis in the orbital space provided by two-orbital flavors, such as

$$|x\rangle \equiv (x^2 - y^2)/\sqrt{2}, \quad |z\rangle \equiv (3z^2 - r^2)/\sqrt{6}, \tag{2.3}$$

and this orbital flavor is in general not conserved along the hopping processes—the orbitals may be changed for the hopping along the bonds in ab planes in the perovskite structure. In this case one obtains

$$t_{ij}^{\alpha\beta} = -\frac{t}{4}\begin{pmatrix} 3 & \pm\sqrt{3} \\ \pm\sqrt{3} & 1 \end{pmatrix}, \tag{2.4}$$

where t stands for an effective $(dd\sigma)$ hopping matrix element. For more details see Refs. 18 and 24. In contrast, for t_{2g} orbitals in a particular plane, there are two degenerate orbitals which are coupled by the hopping $t_{ij}^{\alpha\beta} = -t\delta_{\alpha\beta}$ for the bond $\langle ij \rangle$, so the hopping matrix is diagonal. Here t is the effective $(dd\pi)$ hopping matrix element. In addition, the hopping is one-dimensional (1D), as, for instance, the yz and zx orbitals in ab planes.[25] However, in the two-site cluster model considered below there are two equivalent t_{2g} orbitals which allow for the diagonal hopping, for instance, for yz and zx orbitals along the c axis. Hence, we shall call this case of the degenerate Hubbard model also the t_{2g} orbital model. Eventually, the third one (xy) may be empty, as, for instance, in ab planes of Sr_2VO_4, and therefore neglected.[25]

The electron-electron interaction may be written as follows:[9]

$$\begin{aligned} H_{\rm int} = {} & U_{\rm loc} \sum_i (n_{ix\uparrow} n_{ix\downarrow} + n_{iz\uparrow} n_{iz\downarrow}) + \frac{1}{2} U_{\rm nloc} \sum_{\langle ij \rangle} (n_{ix} + n_{iz}) \\ & \times (n_{jx} + n_{jz}) + \left(U_{\rm loc} - \frac{5}{2} J_H \right) \sum_i n_{ix} n_{iz} - 2J_H \sum_i \vec{S}_{ix} \cdot \vec{S}_{iz} \\ & + J_H \sum_i (c_{ix\uparrow}^{\dagger} c_{ix\downarrow}^{\dagger} c_{iz\downarrow} c_{iz\uparrow} + c_{iz\uparrow}^{\dagger} c_{iz\downarrow}^{\dagger} c_{ix\downarrow} c_{ix\uparrow}). \end{aligned} \tag{2.5}$$

Here $U_{\rm loc}$ and J_H stand for the on-site intraorbital Coulomb and Hund's exchange elements. The energy $U_{\rm nloc}$ represents the intersite Coulomb repulsion, which relevance has been emphasized by several authors,[26–28] especially when addressing molecules. We also used $n_{i\alpha} = \Sigma_\sigma n_{i\alpha\sigma}$ for total electron density operators, given by the sum of densities in orbitals $\alpha = x, z$, defined in Eq. (2.3). Let us here emphasize that this interaction term is spin-rotation invariant and invariant under a rotation around T^y in the orbital space. For e_g electrons, this can be made use of in order to simplify the hopping matrix Eq. (2.4). Indeed, one may introduce the set of orbitals $|\xi\rangle$ and $|\zeta\rangle$ as[18]

$$\begin{pmatrix} |\xi\rangle \\ |\zeta\rangle \end{pmatrix} = e^{-i(\theta/2)\tau_y} \begin{pmatrix} |x\rangle \\ |z\rangle \end{pmatrix}, \tag{2.6}$$

where τ_y is a Pauli matrix. If one uses $\theta = 2\pi/3$, this transformation is equivalent to rotating a two-site molecule along the a axis to a two-site molecule along the c axis. Accordingly the kinetic energy, Eq. (2.2), simplifies into

$$H_{\mathrm{kin}} = -t\sum_{\langle ij\rangle}\sum_{\sigma} c^{\dagger}_{i\zeta\sigma}c_{j\zeta\sigma} \tag{2.7}$$

with the hopping allowed only between the directional orbitals ζ oriented along the bond.

Finally we also consider a uniform CFS between the $|x\rangle$ and $|z\rangle$ orbitals,

$$H_{\mathrm{cf}} = \frac{1}{2}E_0\sum_{i\sigma}(n_{ix\sigma} - n_{iz\sigma}). \tag{2.8}$$

Physically such a splitting may result from a tetragonal Jahn-Teller distortion of MO_6 octahedra, as realized for geometrical reasons in layered manganites,[29] or in the two-dimensional (2D) Sr_2VO_4 compound,[25] or from the $GdFeO_3$-like tilting of MO_6 octahedra in the perovskite structure.[30] Modelwise the combined effect of H_{cf} and H_{int} is shown below to trigger a strong competition between FM and AF ground states and violations of the Goodenough-Kanamori rules, as anticipated in Ref. 19. Here we focus on the quarter-filled band case, where this competition is clearly visible.[10] For a two-site molecule the basis of the Hilbert space is made up of 12 even states and of 16 odd states. Moreover, for each parity, these states can also be distinguished according to the value of the total spin $\vec{\mathcal{S}}=\Sigma_i\vec{S}_i$ and its zth component $\mathcal{S}^z$. We follow below the classification of the states introduced in Ref. 19. The corresponding Hamiltonian matrix can be found in the Appendix.

Let us also emphasize that, while the square of the total spin operator $\vec{\mathcal{S}}$ and its zth component $\mathcal{S}^z$ commute with the Hamiltonian, and can be thus used to label the eigenstates, this does not hold for the total orbital pseudospin operator $\vec{\mathcal{T}}=\Sigma_i\vec{T}_i$, where, at site i, the three components of $\vec{T}_i$ may be defined as follows:

$$T_i^{+} = \sum_{\sigma} c^{\dagger}_{ix\sigma}c_{iz\sigma},$$

$$T_i^{-} = \sum_{\sigma} c^{\dagger}_{iz\sigma}c_{ix\sigma},$$

$$T_i^{z} = \frac{1}{2}\sum_{\sigma}(n_{ix\sigma} - n_{iz\sigma}). \tag{2.9}$$

Accordingly, the CFS term Eq. (2.8), which can be written as

$$H_{\mathrm{cf}} = E_0\mathcal{T}^z = \sum_i T_i^z \tag{2.10}$$

breaks the rotational symmetry in orbital space. For e_g electrons the CFS term takes its simplest form in the $\{|x\rangle,|z\rangle\}$ basis in contrast to the kinetic energy, and hence may play an important role in the competition between the FM and AF ground states.

III. CONSEQUENCES OF HUND'S EXCHANGE

A. Spectrum of the Hamiltonian

Let us now proceed with the diagonalization of the Hamiltonian. While, as shown in the Appendix, this can be performed analytically in the atomic limit ($t=0$), or for vanishing CFS ($E_0=0$), this is not the case anymore for the general models, and we display the 16 different eigenenergies in Fig. 1. The renormalized Coulomb interaction U used in the following is defined in the Appendix, see Eq. (A.4). There are three striking features associated with these spectra.

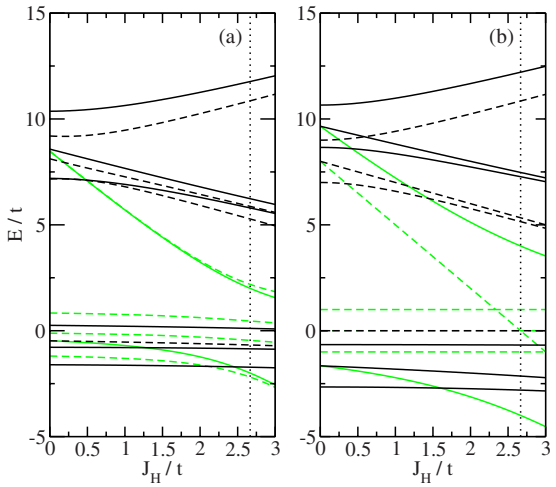

FIG. 1. (Color online) Spectrum of Hamiltonian (2.1) for: (a) e_g electrons and (b) t_{2g} electrons. The full (dashed) black lines correspond to the even (odd) singlet states while the full (dashed) gray (green) lines correspond to the even (odd) triplet states. Parameters: $U=8t$ and $E_0=t$. The vertical dotted lines correspond to $J_H=U/3$ and indicate the limit of the physically relevant regime. For t_{2g} electrons, the lowest odd singlet state is degenerate with the second odd triplet state.

First of all, when increasing the ratio J_H/U (while keeping it smaller than 1/3 to avoid unphysical attractive interactions), the ground state evolves from AF to FM one, both for e_g and t_{2g} model. As will be shown below, the location of this quantum phase transition strongly depends on the value of the CFS. Note that for $J_H=0$ the ground-state energy is close to $-2E_0$ for both models and that it can be further reduced by large J_H.

Second, switching on Hund's exchange interaction affects the high-energy part of the spectra more strongly, in contrast to the ground state. More specifically, when considering the high-energy odd triplet state for both orbitals, its energy decreases with increasing J_H/U as $U-3J_H$, in close analogy to the atomic limit. Regarding the three high-energy odd singlet states, the energy of the upper one increases with increasing J_H. The energies of the other two, which are degenerate for $E_0=0$, roughly decrease as $U-J_H$, as one might anticipate from the atomic limit. Besides, the high-energy even singlet states follow the same trends. Note also that the gap between the low-energy states and the high-energy ones obtained for $J_H=0$ rapidly shrinks with increasing J_H.

B. Magnetic phase diagram

The above discussed competition between FM and AF order in the ground states is summarized in Fig. 2. For e_g electrons and vanishing CFS the FM ground state is only

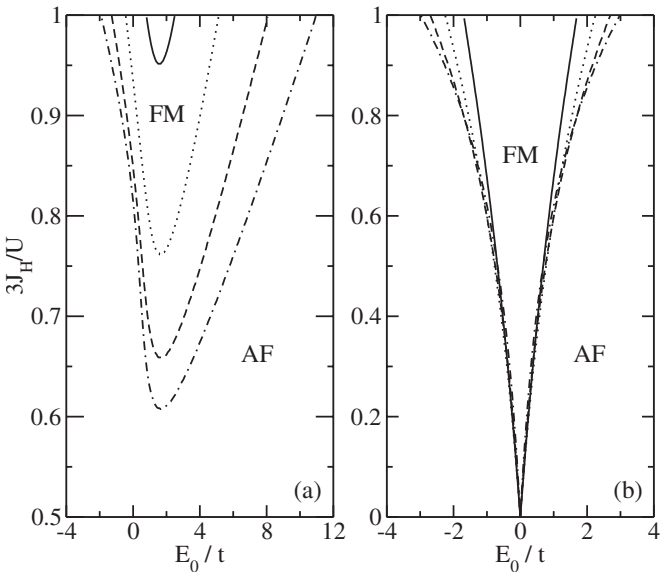

FIG. 2. Magnetic phase diagram obtained in the $\{E_0, J_H\}$ plane from Hamiltonian (2.1) for: (a) e_g electrons and (b) t_{2g} electrons. The full, dotted, dashed, and dashed-dotted lines correspond to $U=5t$, $8t$, $12t$, and $16t$, respectively.

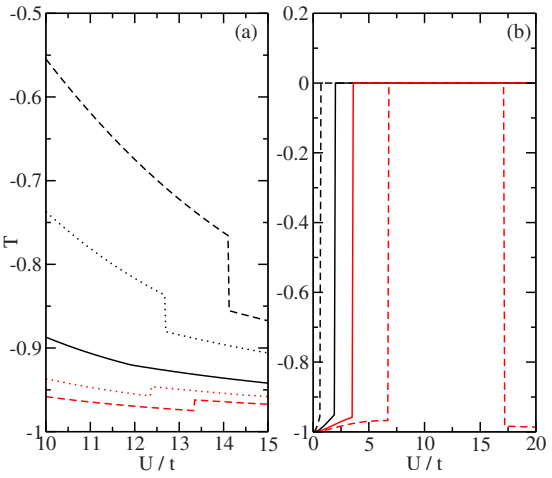

FIG. 3. (Color online) Ground-state orbital polarization for: (a) e_g electrons and $E_0=E_0^{\rm crit}$ (solid line), $E_0=E_0^{\rm crit}-0.5t$ (upper dotted line), $E_0=E_0^{\rm crit}-0.75t$ (upper dashed line), $E_0=E_0^{\rm crit}+0.5t$ (lower dotted line), and $E_0=E_0^{\rm crit}+t$ (lower dashed line), and (b) t_{2g} electrons and $E_0=0.2t$ (left dashed line), $E_0=0.5t$ (left solid line), $E_0=0.8t$ (right solid line), and $E_0=1.1t$ (right dashed lines). Parameter: $J_H/U=0.22$.

stabilized in the vicinity of the physically relevant upper limit of very large Hund's exchange coupling $J_H \simeq U/3$, see Fig. 2(a). The FM domain rapidly vanishes for negative CFS ($E_0<0$). On the contrary, for positive CFS ($E_0>0$), the size of the FM region first rapidly increases with increasing E_0 and the critical J_H above which the ground state is FM can be as small as $U/5$ for ($E_0 \simeq 1.6t$). When E_0 is further increased, the FM region shrinks again and finally vanishes (e.g., at $U=16t$ for large CFS $E_0>11t$). In that case one recovers the AF correlation characterizing the large U regime of the nondegenerate Hubbard model at half filling. In this respect it is worth noting that the relevance of such a model is restricted to values of the CFS larger than U, especially in the large U regime. Altogether, the asymmetry of the magnetic phase diagram between positive and negative values of E_0 reflects the anisotropy of e_g orbitals.

For the degenerate Hubbard model the shape of the phase diagram is quite different, see Fig. 2(b). On top of its symmetry with respect to $E_0=0$, the FM ground state extends down to $J_H=0$ for $E_0=0$. This follows from the diagonal hopping which favors the states with the same spins. The role of an increasing CFS is merely to reduce the range of J_H for which the ground state is FM—AF states occur for large $|E_0|$ due to large amplitude of local singlets (double occupancies) at each site in this regime.

C. Orbital polarization

Another characterization of the above found phase transition is provided by the orbital polarization, which represents the response to the symmetry breaking term represented by the CFS, Eq. (2.10). For t_{2g} electrons the CFS is necessary to induce an orbitally polarized ground state while orbital polarization can spontaneously appear in e_g systems.[10,31,32]

For e_g electrons, the ground state is orbitally polarized, irrespective of the magnetic correlations and the value of the CFS, as shown in Fig. 3(a). For vanishing CFS, the occupancy of the $|z\rangle$ orbital clearly exceeds the one of the $|x\rangle$ orbital, a trend which is enhanced when U is increased in the AF phase. When U is further increased, the magnetic transition takes place and the orbital polarization undergoes a discontinuous jump. The size, and even the sign, of the jump strongly depends on the CFS. For example, for $J_H=0.22U$, we obtain that the jump vanishes for $E_0=E_0^{\rm crit}=1.6675t$ while it is positive and small (negative and substantial) for $E_0>E_0^{\rm crit}$($E_0<E_0^{\rm crit}$). This gives a strong indication that the phase transition is continuous at $E_0^{\rm crit}$ when U increases. This is further supported by the fact that the partial derivative of the ground-state energy with respect to E_0 is also continuous at $E_0^{\rm crit}$. We therefore identified a critical point.

As shown in Fig. 3(b) the situation is qualitatively different for t_{2g} electrons. First of all the phase diagram is symmetric with respect to $E_0=0$. We therefore concentrate on $E_0>0$. Second, a fully orbitally polarized ground state is obtained for an arbitrarily small CFS at $U \simeq 0$. When U is increased $\langle T^z \rangle$ is slightly reduced in the AF phase, and vanishes in the FM phase. Eventually one reenters the AF phase under a further increase in U, here for $E_0 \simeq 1.1t$, in which case the ground state regains its large orbital polarization. Finally, for t_{2g} electrons, the critical point is located at $(E_0, J_H)=(0,0)$, irrespective of the value of U.

IV. OPTICAL CONDUCTIVITY

We now turn to the discussion of the interplay between the magnetic ground state and the optical spectra close to zero temperature. It is well known that magnetic correlations influence the optical spectra in correlated systems[33] and the changes may be quite dramatic in systems with orbital degeneracy.[23]

A. General formalism

Using the Kubo formula the complex optical conductivity $\underline{\sigma}(\omega)$ results as

$$\underline{\sigma}(\omega) = \frac{i}{\omega Z}\sum_{m,n}\frac{e^{-\beta E_m}-e^{-\beta E_n}}{\omega-(\omega_n-\omega_m)+i\eta}|\langle\Psi_m|\hat{\mathrm{J}}_x|\Psi_n\rangle|^2, \quad (4.1)$$

where Z is the canonical partition function and $|\Psi_m\rangle$ is an eigenstate of Hamiltonian (2.1) with eigenenergy E_m, $\beta=1/k_BT$ is inverse temperature, and $\eta>0$ is a small parameter. The above sums run over all eigenstates of $\mathcal{H}$. For the models under consideration the current operator is given by

$$\hat{\mathrm{J}}_x = -ita\sum_{\sigma}(c^+_{1\zeta\sigma}, c^+_{1\xi\sigma})\begin{pmatrix}1 & 0\\ 0 & A\end{pmatrix}\begin{pmatrix}c_{2\zeta\sigma}\\ c_{2\xi\sigma}\end{pmatrix} + \mathrm{H.c.}, \quad (4.2)$$

with $\sigma=\uparrow,\downarrow$, a is the distance between both sites, and either $A=0$ or $A=1$ for e_g and t_{2g} electrons, respectively. This operator couples only states with the same spin projection and with different parities. For our purpose it is convenient to expand the current operator as

$$\hat{\mathrm{J}}_x = \hat{\mathrm{J}}_S + \sum_{m=-1}^{1}\hat{\mathrm{J}}_{T,m} \quad (4.3)$$

with

$$\hat{\mathrm{J}}_S = -ita\{2A|\Phi_3^-\rangle\langle\Phi_4^-| - 2|\Phi_1^-\rangle\langle\Phi_2^-| + (1+A)|\Phi_7^-\rangle\langle\Phi_8^-| + (1-A)|\Phi_7^+\rangle\langle\Phi_8^+|\} + \mathrm{H.c.},$$

$$\hat{\mathrm{J}}_{T,0} = -ita\sum_{\rho=\pm1}(1-A\rho)|\Phi_5^\rho\rangle\langle\Phi_6^\rho| + \mathrm{H.c.},$$

$$\hat{\mathrm{J}}_{T,\pm1} = -ita\sum_{\rho=\pm1}(1-A\rho)|\Psi_{2\pm1}^\rho\rangle\langle\Psi_{1\pm1}^\rho| + \mathrm{H.c.} \quad (4.4)$$

The operator $\hat{\mathrm{J}}_S$ acts on the singlet subspace, while the three operators $\hat{\mathrm{J}}_{T,m}$ couple odd and even triplet states, in their respective subspaces.

According to the above decomposition, the real part of the optical conductivity can be also expanded as

$$\sigma(\omega) = \sigma_S(\omega) + \sum_{m=-1}^{1}\sigma_{T,m}(\omega). \quad (4.5)$$

This form will later on turn out to be very convenient since, depending on the parameter values, the ground state may both belong to the singlet or to the triplet subspaces, in which case the low-temperature optical conductivity is either given by the first or the second contribution. We also note that, when making use of the hermiticity of the current operator, the real part $\sigma(\omega)$ may be written as

$$\sigma(\omega) = \frac{1}{Z}\sum_{E_n>E_m}|\langle\Psi_m|\hat{\mathrm{J}}_x|\Psi_n\rangle|^2(e^{-\beta E_m}-e^{-\beta E_n})F_{mn}(\omega) \quad (4.6)$$

with

$$F_{mn}(\omega) = \frac{4\eta\Omega_{mn}}{(\omega^2-\Omega_{mn}^2-\eta^2)^2+4\omega^2\eta^2}, \quad (4.7)$$

where $\Omega_{mn}=\omega_n-\omega_m=\frac{1}{\hbar}(E_n-E_m)>0$. As the parameter η is small, the functions $F_{mn}(\omega)$ exhibit sharp maxima for $\omega\simeq\Omega_{mn}$, and one finds the amplitude $F_{mn}(\Omega_{mn})\simeq 1/\eta\Omega_{mn}$. One can notice that the matrix representing the current operator is the same in the three triplet subspaces ($m=0,\pm1$), each of them being generated by six states (two even and four odd). Moreover, the three Hamiltonian blocks H_{Tm}^{odd}, on the one hand, and H_{Tm}^{even}, on the other hand, are identical. Therefore the three contributions $\sigma_{T,m}(\omega)$ ($m=0,\pm1$) are identical, yielding $\sigma(\omega)=\sigma_S(\omega)+3\sigma_{T,0}(\omega)$. At high temperature, $\sigma(\omega)$ shows *a priori* 32 different peaks, 24 of them originating from transitions between singlet states, while the remaining eight ones are due to transitions between triplet states. The amplitudes of these peaks depend not only on the value of the matrix elements $\langle\Psi_m|\hat{\mathrm{J}}_x|\Psi_n\rangle$, but also on the statistical weights $(e^{-\beta E_m}-e^{-\beta E_n})/Z$.

B. Influence of the Hund's exchange coupling on the low-temperature optical spectra

At sufficiently low temperature, only the transitions from the ground state contribute to the optical spectrum. Depending on the value of J_H one has to consider two cases. For $J_H<J_H^c$, the ground state is AF and is an eigenstate of the singlet block H_S^{even}, both for e_g and t_{2g} electrons. Accordingly, the real part of the conductivity simplifies into

$$\sigma_S(\omega) = \frac{1}{Z}e^{-\beta E_{\mathrm{AF}}}\sum_m|\langle\Psi_{\mathrm{AF}}|\hat{\mathrm{J}}_S|\Psi_{S,m}^{\mathrm{odd}}\rangle|^2F_{\mathrm{AF},m}(\omega). \quad (4.8)$$

For $J_H>J_H^c$, the ground state is FM. While it possesses odd parity for e_g electrons, it is even for t_{2g} electrons. As a result, in the regime of $J_H>J_H^c$, the low-temperature optical conductivity reduces to

$$\sigma_{T,0}(\omega) \simeq \frac{1}{Z}e^{-\beta E_{\mathrm{FM}}}\sum_m|\langle\Psi_{\mathrm{FM}}|\hat{\mathrm{J}}_{T,0}|\Psi_{T,0,m}^{\mathrm{even}}\rangle|^2F_{\mathrm{FM},m}(\omega), \quad (4.9)$$

for e_g electrons, and to

$$\sigma_{T,0}(\omega) \simeq \frac{1}{Z}e^{-\beta E_{\mathrm{FM}}}\sum_m|\langle\Psi_{\mathrm{FM}}|\hat{\mathrm{J}}_{T,0}|\Psi_{T,0,m}^{\mathrm{odd}}\rangle|^2F_{\mathrm{FM},m}(\omega), \quad (4.10)$$

for t_{2g} electrons. Here m labels the eigenstates resulting from the model Hamiltonian (A.12) and (A.14), respectively. The real part of the conductivity is depicted in Fig. 4 for four representative values of Hund's exchange J_H located in the physical interval $J_H\in[0,U/3]$.

C. Results for e_g electrons

Here we analyze the optical spectra obtained for e_g electrons for increasing value of J_H, see Figs. 4(a)–4(d). First, for $J_H\ll J_H^c$, one notices in Fig. 4(a) that the optical spectra consist of two main peaks. From the position of the maxima it is

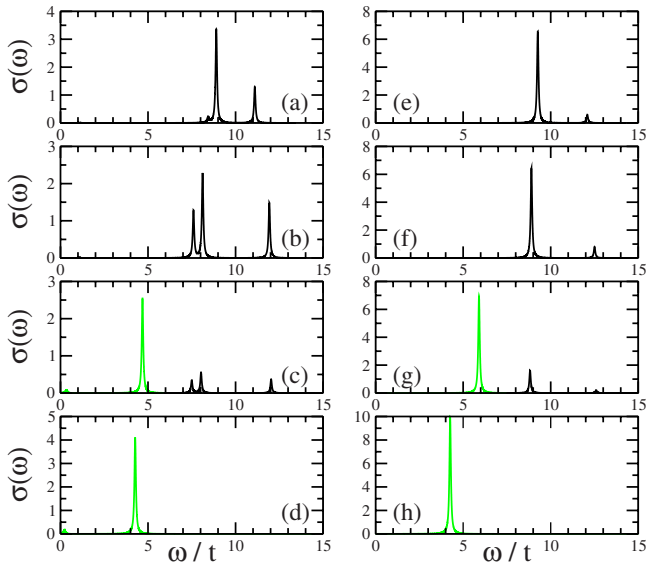

FIG. 4. (Color online) Real part of the optical conductivity $\sigma(\omega)$ at low temperature $\beta t=10^3$ for [(a)–(d)] e_g electrons and [(e)–(h)] t_{2g} electrons, as obtained for increasing values of J_H: [(a) and (e)] $J_H=t$, (b) $J_H=2t$, (f) $J_H=1.5t$, [(c) and (g)] $J_H=J_H^c$, and [(d) and (h)] $J_H=2.5t$. Parameters: $U=8t$, $E_0=t$, and $\eta=0.05$. The black (gray/green) peaks correspond to transitions in the singlet (triplet) subspace.

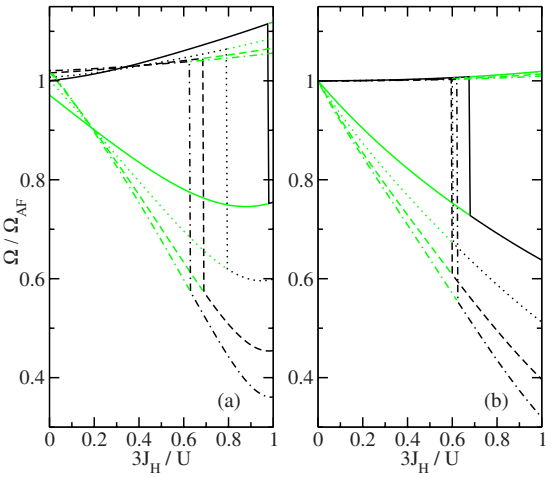

FIG. 5. (Color online) Normalized position of the main peaks Ω in the optical conductivity $\sigma(\omega)$ as obtained in the ground state (black curves) and the first excited state (gray/green curves) for: (a) e_g electrons with $\Omega_{\rm AF}$ given by Eq. (4.11) and (b) t_{2g} electrons with $\Omega_{\rm AF}$ given by Eq. (4.13). Parameter: $E_0=t$. The full, dotted, dashed, and dashed-dotted lines correspond to $U=5t$, $8t$, $12t$, and $16t$, respectively.

possible to unambiguously identify the levels involved in the corresponding optical transitions. According to Fig. 1(a), the two observed transitions occur from the ground state of $H_S^{\rm even}$ toward the second and the third levels of $H_S^{\rm odd}$, represented by dashed black lines in Fig. 1(a). Note that the most pronounced peak corresponds to the third level. In addition, a small contribution resulting from the transition to the first level of $H_S^{\rm odd}$ can also be identified.

When increasing J_H, the main peak both shifts to lower energy and loses its weight, while the second main peak shifts to higher energy and rather gains weight, as shown in Fig. 4(b). Besides, the above-mentioned tiny peak acquires a substantial weight as well. Under a further increase in J_H, the optical spectrum keeps on exhibiting the same qualitative behavior, up to the very vicinity of J_H^c.

For $J_H>J_H^c$, the optical spectrum is manifestly different and consists mainly of a single peak at lower energy, see Fig. 4(d), associated to a transition from the lowest odd triplet state toward the second level of $H_{T0}^{\rm even}$ [full gray/green curve in Fig. 1(a)]. A crossover between this regime and the small J_H one ($J_H<J_H^c$) is found for $J_H\simeq J_H^c$. There, the weight of all transitions from the lowest singlet state is suddenly strongly suppressed and, at J_H^c, it is a transition from the lowest triplet state that dominates the optical spectrum. When $J_H=J_H^c$, the ground state is degenerate, AF and FM contributions are comparable and the optical spectrum at zero temperature consists of four peaks for e_g electrons, see Fig. 4(c). When temperature increases above zero, there appears a finite J_H domain where this feature is robust.

The frequency dependence of the peaks in the optical spectra on J_H can be explained semiquantitatively by considering the eigenvalues of the Hamiltonian given in the Appendix. While it is difficult to discuss analytically the eigenvalues of the Hamiltonian in the singlet subspace, it can be seen in Fig. 1(a) that, in the AF phase, the ground-state energy weakly depends on J_H. In addition, for moderate CFS ($|E_0|\lesssim 1.5t$), it corresponds well to the first excited state for t_{2g} electrons in the same subspace. Regarding the involved excited state, the second excited level of $H_S^{\rm odd}$, its energy is well approximated by $U-J_H$. Hence,

$$\Omega_{\rm AF}\simeq \frac{1}{2}U-J_H+\frac{1}{2}\sqrt{U^2+64t^2}. \tag{4.11}$$

In the FM regime the ground-state energy can be approximated by $\varepsilon_{1,-}$, see Eq. (A.16), while the energy of the excited state of $H_T^{\rm even}$ can be gained from Eq. (A.12). Hence,

$$\Omega_{\rm FM}\simeq \sqrt{(U-3J_H)^2+16t^2}. \tag{4.12}$$

Equations (4.11) and (4.12) hold for larger values of U as well. This behavior explains the drop of the excitation energy by about $2J_H^c$ which can be observed when the Hund's exchange coupling passes through the critical value J_H^c.

For $J_H\simeq J_H^c$ the energy difference between the first excited state and the ground state is small. Accordingly the finite-temperature optical spectra consists of the thermally weighted superposition of excitations in the singlet and triplet subspaces. This, using the results displayed in Fig. 5(a) or following Eqs. (4.11) and (4.12), gives a direct access to J_H, and then to U.

The dependence of the spectral weight of the main peaks in $\sigma(\omega)$ for e_g electrons on J_H and U is displayed in Fig. 6(a). In the AF phase the weight shows little dependence on J_H in the regime of large U while it strongly suppressed for increasing J_H for intermediate values of U. This reflects the J_H dependence of $F_{mn}(\Omega_{mn})\simeq 1/\eta\Omega_{mn}$, see Eq. (4.7), with Ω_{mn} represented in Fig. 5(a), while the matrix elements of the

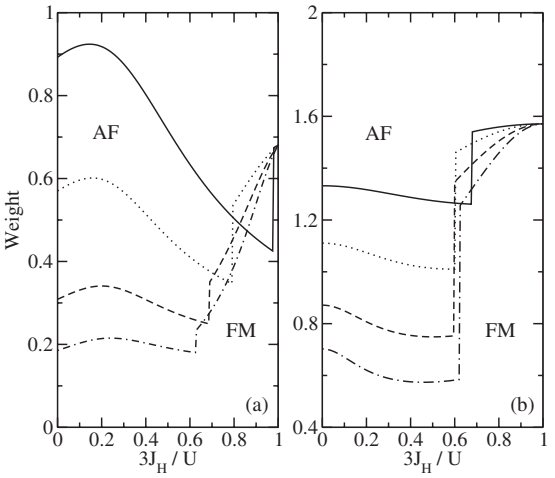

FIG. 6. Weight $\pi\eta\sigma_{\max}$ of the main peaks at $T=0$ for (a) e_g electrons and (b) t_{2g} electrons. Parameters: $E_0=t$ and $\eta=0.05$. The full, dotted, dashed, and dashed-dotted lines correspond to $U=5t$, $8t$, $12t$, and $16t$, respectively.

current are only weakly depending on J_H. In the FM phase Ω_{mn} shows a stronger J_H dependence, which in turn is reflected in the weight. One observes a rapid increase in the spectral weight when J_H increases in the FM configuration beyond $J_H=J_H^c$.

D. Results for t_{2g} electrons

In the case of t_{2g} electrons, one notices in Figs. 4(e) and 4(f) that the optical spectra are dominated by a single peak for small $J_H \ll J_H^c$. According to Fig. 1(b), the transition occurs from the ground state of H_S^{even} toward the second level of H_S^{odd}, as shown by black dashed lines in Fig. 1(b). In addition, a small contribution resulting from the transition to the fourth level of H_S^{odd} can also be noticed. For increasing J_H, the main peak slowly shifts toward smaller energies while its weight remains mostly unaffected. On the contrary, the higher peak gains weight and is shifted toward higher energies.

As already encountered for e_g electrons, the weight of these peaks is dramatically suppressed when J_H is further increased up to J_H^c, and the overwhelming peak follows from the transition involving the lowest triplet state. Under a further increase in J_H, the latter one takes over, its weight increases, while its energy decreases. Note that the transition involves the ground state of H_{T0}^{even} and the fourth level of H_{T0}^{odd}, as depicted in Fig. 1(b). In contrast to the e_g case with four distinct structures at $J_H=J_H^c$ [Fig. 4(c)], one finds here only three maxima [Fig. 4(g)] which follow from the structure of the excited states.

Considering the eigenvalues of the Hamiltonian allows one to explain quite accurately the frequency dependence of the peaks in the optical spectra. First, in the AF phase, the ground-state energy in Fig. 1(b) is seen to depend only very weakly on J_H. It is given by $\varepsilon_{1,-}$, see Eq. (A.7). The energy of the involved excited state is given by $U-\sqrt{E_0^2+J_H^2}$, as can be read off below Eq. (A.9). To a very good approximation we then obtain the involved excitation energies in the AF regime as

$$\Omega_{\text{AF}} \simeq E_0 + \frac{U}{2} - \sqrt{E_0^2 + J_H^2} + \frac{1}{2}\sqrt{U^2 + 64t^2}. \quad (4.13)$$

As shown in Fig. 5, Eqs. (4.11) and (4.13) give a good account of the excitation energies in the AF phase, especially for t_{2g} electrons.

In the FM regime the ground-state energy can be obtained from Eq. (A.12) while the energy of the involved excited state is given by ε_3, see Eq. (A.15). We thus find the exact excitation energies as

$$\Omega_{\text{FM}} = \frac{1}{2}\{U - 3J_H + \sqrt{(U-3J_H)^2 + 64t^2}\}. \quad (4.14)$$

In the vicinity of J_H^c, the above two expressions lead to the following drop of the excitation energy:

$$\delta\Omega = 3J_H - \sqrt{E_0^2 + J_H^2}. \quad (4.15)$$

Thus, for vanishing CFS, this coincides to the result obtained for e_g electrons.

The dependence of the weight of the main peak on J_H is shown in Fig. 6(b) for a few representative values of U. In the AF phase, stable in the regime of low values of J_H, the weight shows little dependence on J_H for both intermediate and large U. This reflects the J_H dependence of $F_{mn}(\Omega_{mn}) \simeq 1/\eta\Omega_{mn}$, see Eq. (4.7), with Ω_{mn} represented in Fig. 5(b), while the matrix elements of the current are only weakly dependent on J_H. In the FM phase Ω_{mn} exhibits a stronger dependence on J_H, which in turn is reflected in the weight, especially for large U. As compared to the e_g electrons case, the jump in the spectral weight at the magnetic transition is here more significant and the values of the spectral weight are considerably larger. This follows from the matrix elements of the current operator in the different ground states.

E. Discussion

In order to discuss the relevance of the above results to lattice problems it seems necessary to perform the calculations for larger clusters as well. Unfortunately the dimension of the Hilbert space increases very rapidly with the cluster size L, and the task is beyond reach for today's computers for $L>10$. Yet, studies of finite-size effects can be better performed in the one-band case. For example, the optical conductivity has been calculated for 4×4 clusters,[34,35] and for 1D chains.[36] At half filling, the optical spectra exhibit a high-frequency broad peak at the energy which corresponds to the upper Hubbard subband. In the two-site approximation the peak loses its width but its position and the spectral weight are rather well reproduced in the regime of large U as it originates from the superexchange determined by charge excitations on individual bonds.[23] It is located at

$$\omega_U = \frac{1}{2}(U + \sqrt{U^2 + 64t^2}) \quad (4.16)$$

using periodic boundary conditions which rescale the hopping from t to $2t$. Analyzing the results obtained by Dagotto

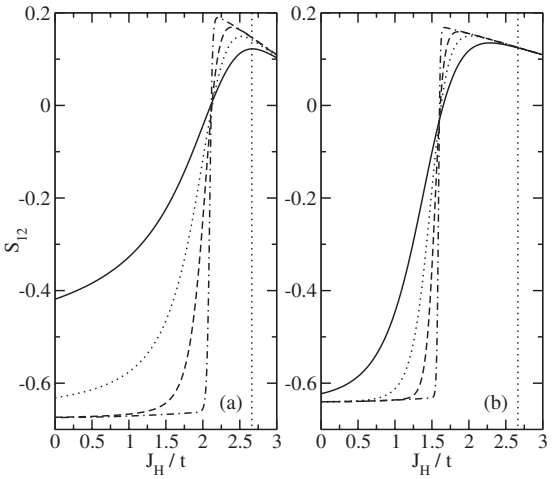

FIG. 7. Intersite spin autocorrelation function S_{12}, Eq. (5.1), as obtained at finite temperature for increasing J_H for: (a) e_g electrons and (b) t_{2g} electrons. Different lines correspond to: $\beta t=5$ (solid lines), $\beta t=10$ (dotted lines), $\beta t=20$ (dashed line, left panel), $\beta t=50$ (dashed line, right panel), and $\beta t=100$ (dashed-dotted lines). Parameters: $U=8t$ and $E_0=t$. The dotted vertical line corresponds to $J_H/U=1/3$.

et al.[34–36] reveals that ω_U quite accurately represents the location of the high-frequency peak, especially in the strong-coupling regime. Hence, we consider that the location of the various high-frequency peaks for the two-orbital models is expected to be given in the lattice case by one of Eqs. (4.11)–(4.14), when appropriate.

V. SPIN AUTOCORRELATION FUNCTION

In order to obtain a complete characterization of the magnetic properties of the considered cluster at finite temperature, we also determined the intersite spin autocorrelation function $S_{12}\equiv\langle\vec{S}_1\cdot\vec{S}_2\rangle$. In the canonical ensemble it may be expressed as

$$S_{12}=\langle\vec{S}_1\cdot\vec{S}_2\rangle=\frac{1}{Z}\sum_m e^{-\beta E_m}\langle\Psi_m|\vec{S}_1\cdot\vec{S}_2|\Psi_m\rangle. \qquad (5.1)$$

Calculations were performed by adding the contributions originating from all subspaces. In Fig. 7 we present the dependence of the thermal average $\langle\vec{S}_1\cdot\vec{S}_2\rangle$, Eq. (5.1), on Hund's exchange J_H for several values of temperature in the physically relevant parameter regime for $U=8t$ and $E_0=t$ (with $t=0.2$ eV the highest temperature for $\beta t=5$ corresponds to ~460 K). Also at finite temperature the change of spin correlations at the critical value of Hund's exchange J_H^c is well visible. For $J_H<J_H^c$, negative $\langle\vec{S}_1\cdot\vec{S}_2\rangle$ reflects the AF nature of the ground state, whereas the correlation between spins becomes FM for $J_H>J_H^c$. As expected, the lower the temperature is, the stiffer the magnetic transition. Remarkably, for e_g electrons, and for small J_H and low temperature, the spin autocorrelation function is close to its limiting value $-3/4$, indicating that double occupancy is here very efficiently suppressed already for this rather moderate value of U. Besides, it is worth noting that, for this moderate value of U, the spin autocorrelation function is far from saturation in the FM regime, and that it even decreases for increasing J_H. These two points are discussed below. One can also notice that all the curves intersect at the same point which confirms that the transition occurs due to level crossing in this system.

Let us characterize more precisely the point of intersection of all the curves for $\langle\vec{S}_1\cdot\vec{S}_2\rangle$ and determine the location of the plateaus which one observes at low temperature in the range of $J_H\ll J_H^c$. With this aim, we denote the lowest two eigenenergies of Hamiltonian (1) as E_{AF} and E_{FM}, and we restrict our considerations to sufficiently low temperatures, so that the relevant contributions to $\langle\vec{S}_1\cdot\vec{S}_2\rangle$ follow only from these lowest eigenstates. For both (e_g and t_{2g}) orbital models, E_{AF} follows from the diagonalization of a single block H_S^{even}. Consequently, E_{AF} appears to be a nondegenerate level. The eigenstate $|\Psi_{\mathrm{AF}}\rangle$ is a linear combination of the basis states belonging to the corresponding six-dimensional subspace.

While the triplet states are threefold degenerate in both (e_g and t_{2g}) cases, the origin of these degenerate values is different. For t_{2g} electrons, the energy E_{FM} comes from the diagonalization of the three identical blocks $H_{T,m}^{\mathrm{even}}$ given by Eq. (A.12), with the lowest energy,

$$E_{\mathrm{FM}}=\frac{1}{2}\{U-3J_H-\sqrt{(U-3J_H)^2+64t^2}\}. \qquad (5.2)$$

Each of the three eigenstates $|\Psi_{\mathrm{FM}}^{(m)}\rangle$ associated to this energy are linear combinations of the basis states belonging to the corresponding 2D subspace. For e_g electrons, E_{FM} is the lowest eigenvalue of the three identical blocks $H_{T,m}^{\mathrm{odd}}$ given by Eq. (A.14).

The particular form of the operators $\vec{S}_1\cdot\vec{S}_2$ (see the Appendix) greatly simplifies the calculation of each contribution. For the AF state one finds,

$$\langle\Psi_{\mathrm{AF}}|\vec{S}_1\cdot\vec{S}_2|\Psi_{\mathrm{AF}}\rangle\equiv-\frac{3}{4}\langle\Psi_{\mathrm{AF}}|\tilde{\mathbf{1}}_{6\times6}^{(3)}|\Psi_{\mathrm{AF}}\rangle=-\frac{3}{4}\langle\tilde{\Psi}_{\mathrm{AF}}|\tilde{\Psi}_{\mathrm{AF}}\rangle, \qquad (5.3)$$

where $|\tilde{\Psi}_{\mathrm{AF}}\rangle$ stands for the ground-state wave function projected onto the singly occupied subspace. In this particular case, it results from the sum of the square modulus of the first three components of the normalized state $|\Psi_{\mathrm{AF}}\rangle$. We further refer to $\langle\tilde{\Psi}_{\mathrm{AF}}|\tilde{\Psi}_{\mathrm{AF}}\rangle$ as the reduced norm.

The contribution of each of the three FM states is

$$\langle\Psi_{\mathrm{FM}}^{(m)}|\vec{S}_1\cdot\vec{S}_2|\Psi_{\mathrm{FM}}^{(m)}\rangle\equiv\frac{1}{4}\langle\tilde{\Psi}_{\mathrm{FM}}^{(m)}|\tilde{\Psi}_{\mathrm{FM}}^{(m)}\rangle. \qquad (5.4)$$

For this state, the reduced norm contains only the first component for t_{2g} electrons and the three first ones for e_g electrons. Due to symmetry, the value of the reduced norm is independent of m. Using these results, the low-temperature intersite spin correlation function can be written as

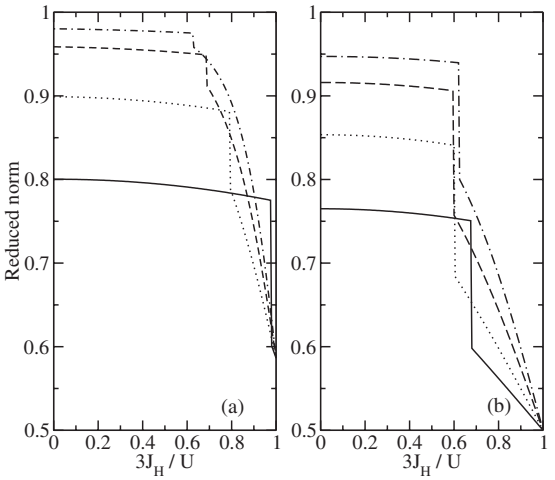

FIG. 8. Reduced norm (see text) obtained for: (a) e_g electrons and (b) t_{2g} electrons. Parameter: $E_0=t$. The full, dotted, dashed, and dashed-dotted lines correspond to $U=5t$, $8t$, $12t$, and $16t$, respectively.

$$\langle \vec{S}_1 \cdot \vec{S}_2 \rangle \simeq \frac{3}{4}\left\{ \frac{-\langle \tilde{\Psi}_{\mathrm{AF}} | \tilde{\Psi}_{\mathrm{AF}} \rangle + e^{-\beta\varepsilon} \langle \tilde{\Psi}^{(0)}_{\mathrm{FM}} | \tilde{\Psi}^{(0)}_{\mathrm{FM}} \rangle}{1+3e^{-\beta\varepsilon}} \right\}, \tag{5.5}$$

where we introduced the excitation energy from the singlet state, $\varepsilon \equiv E_{\mathrm{FM}} - E_{\mathrm{AF}}$. Considering the behavior of the correlation function far from the phase boundary we obtain

$$\langle \vec{S}_1 \cdot \vec{S}_2 \rangle \simeq -\frac{3}{4} \langle \tilde{\Psi}_{\mathrm{AF}} | \tilde{\Psi}_{\mathrm{AF}} \rangle, \tag{5.6}$$

for $J_H \ll J_H^c$ and $\varepsilon > 0$, and

$$\langle \vec{S}_1 \cdot \vec{S}_2 \rangle \simeq \frac{1}{4} \langle \tilde{\Psi}^{(0)}_{\mathrm{FM}} | \tilde{\Psi}^{(0)}_{\mathrm{FM}} \rangle, \tag{5.7}$$

for $J_H \gg J_H^c$ and $\varepsilon < 0$. For t_{2g} electrons in the FM regime, one finds the following analytical expression:

$$\langle \vec{S}_1 \cdot \vec{S}_2 \rangle \simeq \frac{4t^2}{E_{\mathrm{FM}}^2 + 16t^2} \tag{5.8}$$

with E_{FM} given by Eq. (5.2). These results confirm that the ground state is indeed AF for $J_H < J_H^c$ and FM for $J_H > J_H^c$. The reduced norms, $\langle \tilde{\Psi}_{\mathrm{AF}} | \tilde{\Psi}_{\mathrm{AF}} \rangle$ and $\langle \tilde{\Psi}^{(0)}_{\mathrm{FM}} | \tilde{\Psi}^{(0)}_{\mathrm{FM}} \rangle$, obtained for $U=8t$ and $E_0=t$, are shown in Fig. 8. As explained below, one can check that, on the one hand, for $J_H \ll J_H^c$, the AF reduced norm is very close to 1, which yields

$$\langle \vec{S}_1 \cdot \vec{S}_2 \rangle \simeq -\frac{3}{4}, \tag{5.9}$$

and, on the other hand, for $J_H \gg J_H^c$, that the FM reduced norm is lower than one, implying

$$\langle \vec{S}_1 \cdot \vec{S}_2 \rangle < \frac{1}{4}. \tag{5.10}$$

The behavior of these reduced norms, as functions of Hund's exchange J_H, can be explained qualitatively by considering the states which define the blocks H_S^{even}, $H_{T,m}^{\mathrm{even}}$, or $H_{T,m}^{\mathrm{odd}}$.

Let us examine the AF ground state first. For $J_H \ll U$, only the states $\{|\Phi_4^-\rangle, |\Phi_1^-\rangle, |\Phi_8^-\rangle\}$ (one electron per site with opposite spin) contribute to the ground state, while the probabilities (occupancy) of the three remaining states $\{|\Phi_3^+\rangle, |\Phi_2^+\rangle, |\Phi_7^+\rangle\}$ are very small owing to the strong intraorbital Coulomb repulsion. The slight reduction in the AF reduced norm with increasing J_H which can be observed in Fig. 8 is related to the enhancement of the modulus of the $|\Phi_7^+\rangle$ component. This state, built out of local pairs becomes gradually populated due to the decrease of the energy cost $U-J_H$.

Concerning the FM state, the behavior of the reduced norm can be addressed using similar arguments: for large U and low values of J_H, the ground state is predominantly built out of the delocalized states, either $\{|\Psi_{\xi m}\rangle, |\Psi_{\zeta m}\rangle, |\Psi_{1m}^+\rangle\}$ or $\{|\Phi_4^+\rangle, |\Phi_1^+\rangle, |\Phi_6^+\rangle\}$ (one electron per site, triplet states). As J_H increases, the FM reduced norm is stronger suppressed than the AF one because the energy cost of the states $|\Psi_{2m}^-\rangle$ and $|\Phi_5^-\rangle$ (built out of local pairs) is now $U-3J_H$. Therefore, for the same set of parameters, double occupancy is stronger reduced in the AF configuration than in the FM one in the regime of large J_H. As a result, S_{12} will be further away from its saturating value in the FM phase than in the AF one, as seen in Fig. 7.

Finally, we consider the behavior of the correlation function near the level crossing. When the eigenenergies E_{AF} and E_{FM} are very close to one another, one may expand $e^{-\beta\varepsilon}$ to first order in ε, yielding

$$\langle \vec{S}_1 \cdot \vec{S}_2 \rangle \simeq \frac{3}{16}\left\{ \langle \tilde{\Psi}^{(0)}_{\mathrm{FM}} | \tilde{\Psi}^{(0)}_{\mathrm{FM}} \rangle - \langle \tilde{\Psi}_{\mathrm{AF}} | \tilde{\Psi}_{\mathrm{AF}} \rangle - \frac{\beta\varepsilon}{4} \left(3\langle \tilde{\Psi}_{\mathrm{AF}} | \tilde{\Psi}_{\mathrm{AF}} \rangle + \langle \tilde{\Psi}^{(0)}_{\mathrm{FM}} | \tilde{\Psi}^{(0)}_{\mathrm{FM}} \rangle \right) \right\}. \tag{5.11}$$

This formula explains the linear dependence of $\langle \vec{S}_1 \cdot \vec{S}_2 \rangle$ on J_H in the immediate vicinity of the transition at J_H^c, after expanding ε to lowest order in J_H. Furthermore, it shows that when $\varepsilon \to 0$, all the curves have to cross for the same value of

$$\langle \vec{S}_1 \cdot \vec{S}_2 \rangle \simeq \frac{3}{16} \left(\langle \tilde{\Psi}^{(0)}_{\mathrm{FM}} | \tilde{\Psi}^{(0)}_{\mathrm{FM}} \rangle - \langle \tilde{\Psi}_{\mathrm{AF}} | \tilde{\Psi}_{\mathrm{AF}} \rangle \right), \tag{5.12}$$

which vanishes for $U \to \infty$.

VI. ORBITAL AND SPIN-ORBITAL CORRELATIONS

A. Orbital autocorrelation function

Further characterization of the two-site cluster is provided by the orbital and the composite spin-orbital correlation functions. We characterize the orbital pseudospin state at $T=0$ using the intersite orbital autocorrelation function,

$$T_{12} \equiv \langle \vec{T}_1 \cdot \vec{T}_2 \rangle. \tag{6.1}$$

As shown in the Appendix, the matrix elements of the operator $\vec{T}_1 \cdot \vec{T}_2$ strongly resemble the ones of the operator $\vec{S}_1 \cdot \vec{S}_2$.

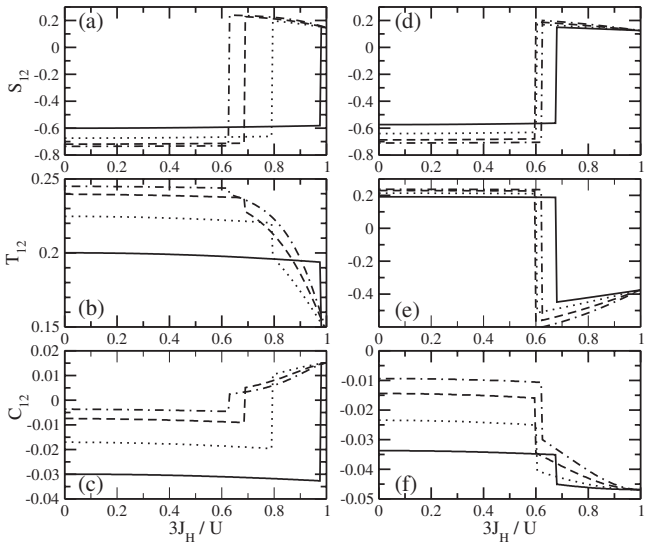

FIG. 9. Low-temperature spin S_{12}, Eq. (5.1), orbital T_{12}, Eq. (6.1), and composite C_{12}, Eq. (6.2) correlation functions for increasing $3J_H/U$, as obtained for: [(a)–(c)] e_g electrons and [(d)–(f)] t_{2g} electrons. The full, dotted, dashed, and dashed-dotted lines in each panel correspond to $U=5t$, $8t$, $12t$, and $16t$, respectively. Parameter: $E_0=t$.

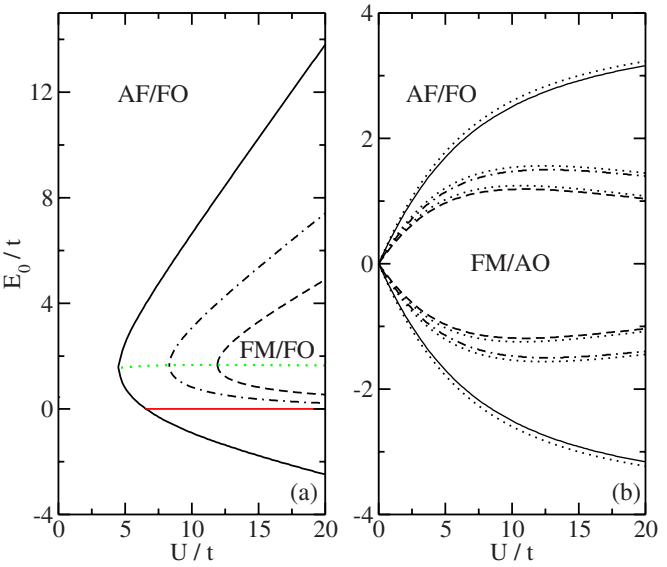

FIG. 10. (Color online) Phase diagram for (a) e_g electrons and (b) t_{2g} electrons at $J_H/U=1/3$ (full lines), 0.25 (dashed-dotted lines), and 0.22 (dashed lines). On the horizontal solid line $E_0=0$ in (a) the lowest odd and even triplet eigenstates are degenerate; along the nearly horizontal dotted (gray/blue) line in (a), and for the corresponding values of J_H approximately given by Eq. (6.6), the phase transition is continuous. In (b), the dotted lines represent the approximate phase boundaries given by Eq. (6.7).

Indeed they are proportional to one another in each subspace but with different coefficients. Therefore, the above discussed magnetic transitions are intimately related to the intersite orbital autocorrelation function but we observed that the actual changes are different for e_g and for t_{2g} electrons.

The magnetic transition for e_g electrons is accompanied by a jump of the orbital correlation function, see Figs. 9(a) and 9(b), but the orbital correlation does not change its sign. Moreover, the amplitude of the jump decreases with increasing U, as both phases are nearly orbitally ordered ferro-orbital (FO) phases. Thus, the Goodenough-Kanamori rules are obeyed here only in the regime of small J_H while in the regime of large J_H they are not. Interestingly, this shows that violation of the Goodenough-Kanamori rules may happen in an itinerant system in the FM phase, in contrast to the strong-coupling (localized) regime,[22] where the spins always decouple from orbitals when the spin order is FM. In contrast, the violation of the Goodenough-Kanamori rules was found before in the spin-orbital $SU(2)\otimes SU(2)$ chain,[37] and in the t_{2g} spin-orbital models for the perovskites,[22] where the AF order coexists with alternating orbital (AO) order in a range of parameters. Here this surprising result could be obtained because FO order of e_g orbitals was selected by the kinetic energy favoring the occupancy of the directional orbitals along the bond which permit the hopping in the 1D system.[38]

For t_{2g} electrons the situation is qualitatively different. As revealed by Figs. 9(d) and 9(e), the magnetic transition is accompanied by an orbital transition, from a nearly orbitally ordered FO phase for small J_H, to a rather disordered AO phase for large J_H. As T_{12} slowly decreases in the AO phase when U increases, a nearly orbitally ordered AO phase will only be realized in the regime of very large U, while the Goodenough-Kanamori rules are obeyed in both magnetic phases.

B. Spin-orbital entanglement

Further information on the nature of spin-orbital state in the involved phases can be gained from the spin-orbital correlation function,[22]

$$C_{12} = \langle (\vec{S}_1 \cdot \vec{S}_2)(\vec{T}_1 \cdot \vec{T}_2) \rangle - \langle \vec{S}_1 \cdot \vec{S}_2 \rangle \langle \vec{T}_1 \cdot \vec{T}_2 \rangle . \qquad (6.2)$$

It quantifies the quality of the mean-field-type decoupling $\langle (\vec{S}_1 \cdot \vec{S}_2)(\vec{T}_1 \cdot \vec{T}_2) \rangle \simeq \langle \vec{S}_1 \cdot \vec{S}_2 \rangle \langle \vec{T}_1 \cdot \vec{T}_2 \rangle$ and vanishes when the above mean-field decoupling becomes exact. Qualitatively it resembles the behavior of S_{12}, however with the important difference that its sign remains unaltered at the magnetic transition for t_{2g} electrons.

Recalling the reduced norms, Eqs. (5.3) and (5.4), allows one to quantify the degree of entanglement of the ground state of the various phases. Indeed, in the AF phases we get

$$C_{12} \simeq \frac{3}{16} \langle \tilde{\Psi}_{\rm AF} | \tilde{\Psi}_{\rm AF} \rangle (\langle \tilde{\Psi}_{\rm AF} | \tilde{\Psi}_{\rm AF} \rangle - 1), \qquad (6.3)$$

for both models. In the FM phase one finds for e_g electrons,

$$C_{12}^e \simeq \frac{1}{16} \langle \tilde{\Psi}_{\rm FM}^{(0)} | \tilde{\Psi}_{\rm FM}^{(0)} \rangle (1 - \langle \tilde{\Psi}_{\rm FM}^{(0)} | \tilde{\Psi}_{\rm FM}^{(0)} \rangle) \qquad (6.4)$$

and for t_{2g} electrons,

$$C_{12}^t \simeq \frac{3}{16} \langle \tilde{\Psi}_{\rm FM}^{(0)} | \tilde{\Psi}_{\rm FM}^{(0)} \rangle (\langle \tilde{\Psi}_{\rm FM}^{(0)} | \tilde{\Psi}_{\rm FM}^{(0)} \rangle - 1). \qquad (6.5)$$

Using these relations, it is easy to show that C_{12} neither vanishes in the AF phase nor in the FM one in the regime of finite U, though its magnitude clearly decreases in the AF

phase with increasing U, and weakly decreases in the FM phase, as shown in Figs. 9(c) and 9(f). This behavior is different from the one found in the spin-orbital superexchange models, where spin and orbital operators factorize in FM states.[22]

A summary of the above discussed phase transitions is presented in Fig. 10. Here we plot the phase diagram for both models in the (E_0, U) plane for several values of J_H/U. As seen in Fig. 10(a) for e_g orbitals and $J_H=U/3$, the size of the FM region increases linearly with U for large U, while it closes rather abruptly for $U\simeq 5t$. In this respect, ferromagnetism appears as a strong-coupling property, as already emphasized by several authors in various context.[39] When reducing the ratio J_H/U the FM region gradually shrinks around $E_0\simeq 1.66t$ and is pushed toward larger U. Remarkably, we found that in this case FM order coexists with FO order for large values of J_H, quantum fluctuations are quenched, and the Goodenough-Kanamori rule predicting the complementary behavior of spin and orbital correlations is violated.

Regarding the critical point it is exactly located at the left tip of the FM/FO lobe. $E_0^{\rm crit}$ shows little dependence on U, being, for instance, $1.57t$ for $U=5t$ and $1.64t$ for $U=20t$, while we numerically determined $J_H^{\rm crit}$ to be very well approximated by

$$J_H^{\rm crit}\simeq 0.15U+0.83t. \tag{6.6}$$

On the contrary, for the degenerate Hubbard model and $J_H=U/3$, the phase boundary saturates to $E_0=\pm 4t$ for large U, and extends to zero for $U\to 0$. When reducing the ratio J_H/U the FM region also gradually shrinks but around $E_0=0$. Also, the phase boundary passes over a maximum, which is directly linked with the re-entrant behavior of $\langle T^z\rangle$ encountered in Fig. 3(b). Nevertheless the phase boundary still extends to $E_0=0$ for $U\to 0$.

For t_{2g} electrons, the phase boundary associated with a given J_H can be approximately obtained in the following fashion: in the triplet even subspace, the ground-state energy can be obtained in analytical form by diagonalizing the Hamiltonian matrix Eq. (A.12), while Fig. 1(b) shows that the singlet even ground-state energy weakly depends on J_H. Hence, it is well approximated by $\varepsilon_{1,-}$ for $E_0>0$ (and by $\varepsilon_{3,-}$ for $E_0<0$) given by Eq. (A.7). Solving the resulting equation for the phase boundary with respect to $E_0^{\rm crit}$ yields

$$E_0^{\rm crit}=\pm\frac{1}{2}(3J_H-\sqrt{U^2+64t^2}+\sqrt{(U-3J_H)^2+64t^2}). \tag{6.7}$$

It is represented in Fig. 10(b), which shows that the agreement with the exact result is very good. In particular, this approximate phase boundary also extends to $E_0=0$ for vanishing U. While this is a generic property of the degenerate Hubbard model, following from the SU(4) symmetry at that point, the location of the critical point for e_g orbitals is likely to be somewhat different for larger systems or different geometries. Yet, for both models, these phase boundaries coincide with the ones resulting from strong-coupling expansion for the chain case in the large-U limit.

VII. DISCUSSION AND SUMMARY

The present study provides further evidence that optical spectra are intimately related to the magnetic properties in strongly correlated electron systems. When FM states are stabilized for relatively large values of J_H, the high-spin charge excitations lead to peaks in the optical conductivity at energies $\sim U-3J_H$. In contrast, the low-spin excitations active in the AF phase result into peaks in the optical conductivity at energies $\sim U-J_H$ (or higher). The AF states occur at lower values of J_H than their FM counterparts. This implies the spectral weight transfer from high to low energies under increasing J_H. Interestingly, in the crossover regime between these two types of magnetic order, the excitations characteristic for both phases were obtained. Although the parameter J_H is not directly accessible in a single experiment, by varying temperature one will redistribute the spectral weight over the low-spin and high-spin excitations, as observed, for instance, in the optical spectroscopy for $LaVO_3$,[40] $LaMnO_3$,[41] as well as for $YTiO_3$ and $SmTiO_3$.[42] This, together with Fig. 5 or Eqs. (4.11)–(4.14), thus provides a way to estimate both U and J_H experimentally.

We would like to emphasize the advantage of the suggested procedure of deducing the effective parameters from experiment rather than, as done frequently, from the LDA+DMFT calculations. In fact, the meaning of these parameters is transparent in a model Hamiltonian and they are inherently associated to a given Hamiltonian.[43] Therefore, the effective parameters deduced from experiment are frequently reduced as compared with their values used in the LDA+DMFT calculations. For instance, in $LaMnO_3$ one finds from the optical spectra $U=3.1$ eV and $J_H=0.6$ eV,[41] while these parameters deduced from the LDA+DMFT calculations are: $U=5$ eV and $J_H=0.75$ eV.[44]

Finally, by looking at the phase diagrams of Figs. 2 and 10, we conclude that the FM states can be realized more easily in case of t_{2g} electrons than in case of e_g ones. The range of FM states is broader for t_{2g} electrons and the FM state is favored for degenerate t_{2g} orbitals already for infinitesimal values of $J_H>0$. It may be expected that easier FM polarization in t_{2g} electron systems could survive in the thermodynamic limit, while in e_g systems electrons may change the orbitals and the kinetic energy is larger for the same value of the hopping t, so the conditions for FM states are there also less favorable,[18] although we have shown that a moderate positive crystal field splitting can also trigger a FM ground state. We have also found that in this case FM order coexists with FO order for large values of J_H, and the Goodenough-Kanamori rule predicting the complementary behavior of spin and orbital correlations is violated. It remains a challenge to search for a transition-metal oxide system that could serve as an experimental example of this behavior.

ACKNOWLEDGMENTS

We thank T. Kopp, S. Kremer, T. Pruschke, M. Raczkowski, K. Rościszewski, and Ch. Simon for insightful discussions. P.B., M.H., and R.F. gratefully acknowledge the Région Basse-Normandie and the Ministère de la Recherche

for financial support. A.M.O. acknowledges support by the Foundation for Polish Science (FNP) and by the Polish Ministry of Science and Higher Education under Project No. N202 104138.

APPENDIX: EXACT SOLUTION FOR TWO ELECTRONS

Here we derive the Hamiltonian matrix in the two-particle subspace, as well as that part of the spectrum that can be brought to a simple analytical form. We also derive the matrix elements of the operators $\vec{S}_1 \cdot \vec{S}_2$ and $\vec{T}_1 \cdot \vec{T}_2$, adopting the notation introduced in Ref. 19. Since the Hamiltonian commutes with the parity operator and the spin operators $\mathbf{S}^2$ and S^z, the Hilbert space decomposes into one even and one odd $S=0$ subspaces, and into three even and three odd $S=1$ subspaces. In order to simplify the notation we introduce $E_c=-E_0/2$ and $E_s=\sqrt{6}E_0/4$, the hopping parameters $t_{\xi\xi}=(t_+-t_-)/2$, and $t_{\zeta\zeta}=(t_++t_-)/2$, as well as $t_+=t_-=2t$ for e_g orbitals and $t_+=4t, t_-=0$ for t_{2g} orbitals.

1. Direct Coulomb interaction

For a two-site molecule with periodic boundary conditions, the nonlocal term has to account for the interaction of a given electron with those located on the two neighboring sites. Hence, in each of the four n-dimensional subspaces introduced above, the matrix elements of the direct on-site and intersite Coulomb interaction may be written as

$$H_C^d = U_{\mathrm{loc}}(\mathbf{1}_{n\times n} - \tilde{\mathbf{1}}^{(p)}_{n\times n}) + 2U_{\mathrm{nloc}}\tilde{\mathbf{1}}^{(p)}_{n\times n}, \tag{A.1}$$

where $\mathbf{1}_{n\times n}$ is the n-dimensional identity matrix. The truncated identity matrix $\tilde{\mathbf{1}}^{(p)}_{n\times n}$ is a diagonal $n\times n$ matrix, the first p diagonal matrix elements of which are one, while the $n-p$ remaining ones are zero. It represents the projector on the subspace involving singly occupied sites only, and may be expressed as

$$(\tilde{\mathbf{1}}^{(p)}_{n\times n})_{ij} = \sum_{k=1}^{p} \delta_{i,k}\delta_{j,k}. \tag{A.2}$$

Writing the above matrix elements in the form

$$H_C^d = 2U_{\mathrm{nloc}}\mathbf{1}_{n\times n} + (U_{\mathrm{loc}} - 2U_{\mathrm{nloc}})(\mathbf{1}_{n\times n} - \tilde{\mathbf{1}}^{(p)}_{n\times n}), \tag{A.3}$$

shows that the intersite Coulomb interaction can simply be taken into account by renormalizing the on-site one,

$$U = U_{\mathrm{loc}} - 2U_{\mathrm{nloc}}, \tag{A.4}$$

and by shifting the zero of energy by $2U_{\mathrm{nloc}}$. Note that this shift of origin has no impact on the correlation functions. As $|U_{\mathrm{nloc}}| \ll U_{\mathrm{loc}}$ is often realized in a solid, we use here the symbol U for the renormalized on-site interaction.

2. Singlet even subspace

Using periodic boundary conditions and $\{|\Phi_4^-\rangle, |\Phi_1^-\rangle, |\Phi_8^-\rangle, |\Phi_3^+\rangle, |\Phi_2^+\rangle, |\Phi_7^+\rangle\}$ as a basis of the even singlet subspace we obtain

$$H_S^{\mathrm{even}} = \begin{pmatrix} E_c & 0 & E_s & 2t_{\xi\xi} & 0 & 0 \\ 0 & -E_c & E_s & 0 & 2t_{\zeta\zeta} & 0 \\ E_s & E_s & 0 & 0 & 0 & t_+ \\ 2t_{\xi\xi} & 0 & 0 & E_c+U & J_H & E_s \\ 0 & 2t_{\zeta\zeta} & 0 & J_H & -E_c+U & E_s \\ 0 & 0 & t_+ & E_s & E_s & U-J_H \end{pmatrix}. \tag{A.5}$$

Remarkably, for t_{2g} electrons, two eigenvalues of H_S^{even} can be obtained in a simple analytical form. They read $(U-J_H \pm \sqrt{(U-J_H)^2+64t^2})/2$ and correspond to the second and fifth lowest states. In the atomic limit the spectrum simplifies to $\{-E_0, 0, E_0, U-\sqrt{J_H^2+E_0^2}, U-J_H, U+\sqrt{J_H^2+E_0^2}\}$ while for vanishing CFS it reads

$$\varepsilon_{1,\pm} = \frac{1}{2}(U - J_H \pm \sqrt{(U-J_H)^2+64t^2}),$$

$$\varepsilon_{2,\pm} = \frac{1}{2}(U + J_H \pm \sqrt{(U+J_H)^2+64t^2}), \tag{A.6}$$

with the first two eigenvalues $\varepsilon_{1,\pm}$ being twofold degenerate.

For $J_H=0$ the six eigenenergies can also be obtained in analytical form

$$\varepsilon_{1,\pm} = \frac{1}{2}(U - 2E_0 \pm \sqrt{U^2+64t^2}),$$

$$\varepsilon_{2,\pm} = \frac{1}{2}(U \pm \sqrt{U^2+64t^2}),$$

$$\varepsilon_{3,\pm} = \frac{1}{2}(U + 2E_0 \pm \sqrt{U^2+64t^2}). \tag{A.7}$$

For e_g electrons, none of the eigenvalues of H_S^{even} can be obtained in a simple analytical form in the general case. In the atomic limit the spectrum coincides with the above spectrum for t_{2g} electrons while for vanishing CFS three simple eigenvalues read $\{(U-J_H-\sqrt{(U-J_H)^2+16t^2})/2, 0, (U-J_H+\sqrt{(U-J_H)^2+16t^2})/2\}$.

Regarding the matrix elements of $\vec{S}_1 \cdot \vec{S}_2$ and $\vec{T}_1 \cdot \vec{T}_2$ we obtain in this subspace,

$$\vec{S}_1 \cdot \vec{S}_2 = -3\vec{T}_1 \cdot \vec{T}_2 = -\frac{3}{4}\tilde{\mathbf{1}}^{(3)}_{6\times 6}. \tag{A.8}$$

3. Singlet odd subspace

Using $\{|\Phi_8^+\rangle, |\Phi_3^-\rangle, |\Phi_2^-\rangle, |\Phi_7^-\rangle\}$ as a basis of the odd singlet subspace we obtain

$$H_S^{\mathrm{odd}} = \begin{pmatrix} 0 & 0 & 0 & t_- \\ 0 & E_c+U & J_H & E_s \\ 0 & J_H & -E_c+U & E_s \\ t_- & E_s & E_s & U-J_H \end{pmatrix}. \tag{A.9}$$

For t_{2g} electrons, the spectrum reads: $\{0, U-\sqrt{E_0^2+J_H^2}, U-J_H, U+\sqrt{E_0^2+J_H^2}\}$. For e_g electrons, none of the eigenval-

ues of H_S^{even} can be obtained in a simple analytical form in the general case. In the atomic limit the spectrum coincides with the above one for t_{2g} electrons while for vanishing CFS it reads

$$\varepsilon_{1,\pm} = \frac{1}{2}(U - J_H \pm \sqrt{(U - J_H)^2 + 16t^2}),$$

$$\varepsilon_{2,\pm} = U \pm J_H. \tag{A.10}$$

In this subspace the matrix elements of $\vec{S}_1 \cdot \vec{S}_2$ and $\vec{T}_1 \cdot \vec{T}_2$ operators are given by

$$\vec{S}_1 \cdot \vec{S}_2 = \vec{T}_1 \cdot \vec{T}_2 = -\frac{3}{4}\tilde{\mathbf{1}}_{4\times 4}^{(1)}. \tag{A.11}$$

4. Triplet even subspace

Using the eigenstates of S_z (with eigenvalue 0) $\{|\Phi_6^-\rangle, |\Phi_5^+\rangle\}$ as a basis of the even triplet subspace we obtain

$$H_{T,m}^{\text{even}} = \begin{pmatrix} 0 & t_+ \\ t_+ & U - 3J_H \end{pmatrix}. \tag{A.12}$$

The very same matrix would have been found had we chosen either the eigenstates of S_z (with eigenvalue 1) $\{|\Psi_{1\uparrow}^-\rangle, |\Psi_{2\uparrow}^+\rangle\}$ or the eigenstates of S_z (with eigenvalue −1) $\{|\Psi_{1\downarrow}^-\rangle, |\Psi_{2\downarrow}^+\rangle\}$ as basis. The matrix elements of the operators $\vec{S}_1 \cdot \vec{S}_2$ and $\vec{T}_1 \cdot \vec{T}_2$ in this subspace read

$$\vec{S}_1 \cdot \vec{S}_2 = -\frac{1}{3}\vec{T}_1 \cdot \vec{T}_2 = \frac{1}{4}\tilde{\mathbf{1}}_{2\times 2}^{(1)}. \tag{A.13}$$

5. Triplet odd subspace

Using the S_z eigenstates (with eigenvalue 0) $\{|\Phi_4^+\rangle, |\Phi_1^+\rangle, |\Phi_6^+\rangle, |\Phi_5^-\rangle\}$ as a basis of the odd triplet subspace we obtain

$$H_{T,m}^{\text{odd}} = \begin{pmatrix} E_c & 0 & E_s & 0 \\ 0 & -E_c & E_s & 0 \\ E_s & E_s & 0 & t_- \\ 0 & 0 & t_- & U - 3J_H \end{pmatrix}. \tag{A.14}$$

Again, choosing the eigenstates of S_z (with eigenvalue 1) $\{|\Psi_{\xi\uparrow}\rangle, |\Psi_{\zeta\uparrow}\rangle, |\Psi_{1\uparrow}^+\rangle, |\Psi_{2\uparrow}^-\rangle\}$ or the eigenstates of S_z (with eigenvalue −1) $\{|\Psi_{\xi\downarrow}\rangle, |\Psi_{\zeta\downarrow}\rangle, |\Psi_{1\downarrow}^+\rangle, |\Psi_{2\downarrow}^-\rangle\}$ as basis delivers the same answer. Let us notice that, for t_{2g} electrons, the eigenvalues are given by

$$\varepsilon_{1,\pm} = \pm E_0,$$

$$\varepsilon_2 = 0,$$

$$\varepsilon_3 = U - 3J_H, \tag{A.15}$$

while no simple analytical form can be obtained for e_g electrons in the general case. Still, the same spectrum is obtained in the atomic limit, while, for vanishing CFS, the spectrum reads

$$\varepsilon_{1,\pm} = \frac{1}{2}(U - 3J_H \pm \sqrt{(U - 3J_H)^2 + 16t^2}),$$

$$\varepsilon_2 = 0, \tag{A.16}$$

with the energy ε_2 being twofold degenerate. Regarding the matrix elements of $\vec{S}_1 \cdot \vec{S}_2$ and $\vec{T}_1 \cdot \vec{T}_2$ operators we obtain in this subspace,

$$\vec{S}_1 \cdot \vec{S}_2 = \vec{T}_1 \cdot \vec{T}_2 = \frac{1}{4}\tilde{\mathbf{1}}_{4\times 4}^{(3)}. \tag{A.17}$$

Remarkably, in the limit of vanishing CFS, the lowest 2×2 block of the Hamiltonian matrix, Eq. (A.14), and the Hamiltonian matrix, Eq. (A.12), are identical for e_g orbitals. This leads to a higher symmetry of the ground state along the red line in Fig. 10(a) and possibly to richer optical spectra. Yet it turns out not to be the case, as the matrix elements of the current operator between the lowest even triplet state and the two intermediate odd triplet states vanish. Accordingly this higher symmetry has no genuine impact on the optical conductivity.

[1] G. Kotliar, S. Y. Savrasov, K. Haule, V. S. Oudovenko, O. Parcollet, and C. A. Marianetti, Rev. Mod. Phys. **78**, 865 (2006).

[2] K. Held, G. Keller, V. Eyert, D. Vollhardt, and V. I. Anisimov, Phys. Rev. Lett. **86**, 5345 (2001); F. Rodolakis, P. Hansmann, J.-P. Rueff, A. Toschi, M. W. Haverkort, G. Sangiovanni, A. Tanaka, T. Saha-Dasgupta, O. K. Andersen, K. Held, M. Sikora, I. Alliot, J.-P. Itié, F. Baudelet, P. Wzietek, P. Metcalf, and M. Marsi, *ibid.* **104**, 047401 (2010).

[3] G. Keller, K. Held, V. Eyert, D. Vollhardt, and V. I. Anisimov, Phys. Rev. B **70**, 205116 (2004).

[4] A. I. Poteryaev, J. M. Tomczak, S. Biermann, A. Georges, A. I. Lichtenstein, A. N. Rubtsov, T. Saha-Dasgupta, and O. K. Andersen, Phys. Rev. B **76**, 085127 (2007).

[5] Y. Otsuka and M. Imada, J. Phys. Soc. Jpn. **75**, 124707 (2006).

[6] S. Savrasov, G. Kotliar, and E. Abrahams, Nature (London) **410**, 793 (2001).

[7] J. Zaanen and G. A. Sawatzky, J. Solid State Chem. **88**, 8 (1990).

[8] M. Raczkowski, R. Frésard, and A. M. Oleś, Phys. Rev. B **73**, 094429 (2006).

[9] A. M. Oleś, Phys. Rev. B **28**, 327 (1983).

[10] R. Frésard, M. Raczkowski, and A. M. Oleś, Phys. Status Solidi

B **242**, 370 (2005).
[11] A. Romano, C. Noce, and M. E. Amendola, J. Phys.: Condens. Matter **20**, 465216 (2008).
[12] R. Peters and T. Pruschke, Phys. Rev. B **81**, 035112 (2010).
[13] S. Raghu, X.-L. Qi, C.-X. Liu, D. J. Scalapino, and S.-C. Zhang, Phys. Rev. B **77**, 220503 (2008); A. Moreo, M. Daghofer, J. A. Riera, and E. Dagotto, *ibid.* **79**, 134502 (2009).
[14] Y. Imai and N. Kawakami, J. Phys. Soc. Jpn. **70**, 2365 (2001).
[15] C. Knecht, N. Blümer, and P. G. J. van Dongen, Phys. Rev. B **72**, 081103 (2005); L. de'Medici, A. Georges, and S. Biermann, *ibid.* **72**, 205124 (2005).
[16] H. Lee, Y.-Z. Zhang, H. O. Jeschke, R. Valentí, and H. Monien, Phys. Rev. Lett. **104**, 026402 (2010).
[17] T. Kita, T. Ohashi, and S.-i. Suga, Phys. Rev. B **79**, 245128 (2009).
[18] L. F. Feiner and A. M. Oleś, Phys. Rev. B **71**, 144422 (2005).
[19] M. Raczkowski, R. Frésard, and A. M. Oleś, J. Phys.: Condens. Matter **18**, 7449 (2006).
[20] J. Chaloupka and G. Khaliullin, Phys. Rev. Lett. **100**, 016404 (2008).
[21] J. Kanamori, J. Phys. Chem. Solids **10**, 87 (1959); J. B. Goodenough, *Magnetism and the Chemical Bond* (Wiley-Interscience, New York, 1963).
[22] A. M. Oleś, P. Horsch, L. F. Feiner, and G. Khaliullin, Phys. Rev. Lett. **96**, 147205 (2006).
[23] G. Khaliullin, P. Horsch, and A. M. Oleś, Phys. Rev. B **70**, 195103 (2004); A. M. Oleś, G. Khaliullin, P. Horsch, and L. F. Feiner, *ibid.* **72**, 214431 (2005).
[24] J. C. Slater and G. F. Koster, Phys. Rev. **94**, 1498 (1954).
[25] M. Daghofer, K. Wohlfeld, A. M. Oleś, E. Arrigoni, and P. Horsch, Phys. Rev. Lett. **100**, 066403 (2008); K. Wohlfeld, M. Daghofer, A. M. Oleś, and P. Horsch, Phys. Rev. B **78**, 214423 (2008); K. Wohlfeld, A. M. Oleś, and P. Horsch, *ibid.* **79**, 224433 (2009).
[26] P. Pou, R. Pérez, F. Flores, A. Levy Yeyati, A. Martin-Rodero, J. M. Blanco, F. J. García-Vidal, and J. Ortega, Phys. Rev. B **62**, 4309 (2000).
[27] J. E. Hirsch, Phys. Rev. B **65**, 184502 (2002).
[28] G. Chiappe, E. Louis, E. SanFabián, and J. A. Vergés, Phys. Rev. B **75**, 195104 (2007).
[29] M. Daghofer, A. M. Oleś, D. M. Neuber, and W. von der Linden, Phys. Rev. B **73**, 104451 (2006); M. Daghofer and A. M. Oleś, Acta Phys. Pol. A **111**, 497 (2007); K. Rościszewski and A. M. Oleś, J. Phys.: Condens. Matter **20**, 365212 (2008).
[30] M. Mochizuki and M. Imada, J. Phys. Soc. Jpn. **73**, 1833 (2004); E. Pavarini, Y. Yamasaki, J. Nuss, and O. K. Andersen, New J. Phys. **7**, 188 (2005).
[31] F. Mack and P. Horsch, Phys. Rev. Lett. **82**, 3160 (1999); J. Bała, P. Horsch, and F. Mack, Phys. Rev. B **69**, 094415 (2004); J. Bała and P. Horsch, *ibid.* **72**, 012404 (2005).
[32] A. Koizumi, S. Miyaki, Y. Kakutani, H. Koizumi, N. Hiraoka, K. Makoshi, N. Sakai, K. Hirota, and Y. Murakami, Phys. Rev. Lett. **86**, 5589 (2001).
[33] M. Aichhorn, P. Horsch, W. von der Linden, and M. Cuoco, Phys. Rev. B **65**, 201101 (2002).
[34] E. Dagotto, A. Moreo, F. Ortolani, D. Poilblanc, and J. Riera, Phys. Rev. B **45**, 10741 (1992).
[35] J. A. Riera and E. Dagotto, Phys. Rev. B **50**, 452 (1994).
[36] H. Eskes and A. M. Oleś, Phys. Rev. Lett. **73**, 1279 (1994); H. Eskes, A. M. Oleś, M. B. J. Meinders, and W. Stephan, Phys. Rev. B **50**, 17980 (1994).
[37] A. M. Oleś, P. Horsch, and G. Khaliullin, Phys. Status Solidi B **244**, 2378 (2007).
[38] M. Daghofer, A. M. Oleś, and W. von der Linden, Phys. Rev. B **70**, 184430 (2004).
[39] C. Lacroix-Lyon-Caen and M. Cyrot, Solid State Commun. **21**, 837 (1977); K. Held and D. Vollhardt, Phys. Rev. Lett. **84**, 5168 (2000); R. Frésard and M. Lamboley, J. Low Temp. Phys. **126**, 1091 (2002); M. Stier and W. Nolting, Phys. Rev. B **75**, 144409 (2007); H. Park, K. Haule, C. A. Marianetti, and G. Kotliar, *ibid.* **77**, 035107 (2008).
[40] S. Miyasaka, Y. Okimoto, and Y. Tokura, J. Phys. Soc. Jpn. **71**, 2086 (2002).
[41] N. N. Kovaleva, A. V. Boris, C. Bernhard, A. Kulakov, A. Pimenov, A. M. Balbashov, G. Khaliullin, and B. Keimer, Phys. Rev. Lett. **93**, 147204 (2004); N. N. Kovaleva, A. M. Oleś, A. M. Balbashov, A. Maljuk, D. N. Argyriou, G. Khaliullin, and B. Keimer, Phys. Rev. B **81**, 235130 (2010).
[42] A. Gössling, R. Schmitz, H. Roth, M. W. Haverkort, T. Lorenz, J. A. Mydosh, E. Müller-Hartmann, and M. Grüninger, Phys. Rev. B **78**, 075122 (2008).
[43] J. A. Vergés, E. SanFabián, G. Chiappe, and E. Louis, Phys. Rev. B **81**, 085120 (2010).
[44] A. Yamasaki, M. Feldbacher, Y.-F. Yang, O. K. Andersen, and K. Held, Phys. Rev. Lett. **96**, 166401 (2006); Y.-F. Yang and K. Held, Phys. Rev. B **76**, 212401 (2007).